Cell Reports, Volume *43*

Supplemental information

Homeostatic coordination of cellular phosphate uptake and efflux requires an organelle-based receptor for the inositol pyrophosphate IP8

Xingyao Li, Regan B. Kirkpatrick, Xiaodong Wang, Charles J. Tucker, Anuj Shukla, Henning J. Jessen, Huanchen Wang, Stephen B. Shears, and Chunfang Gu

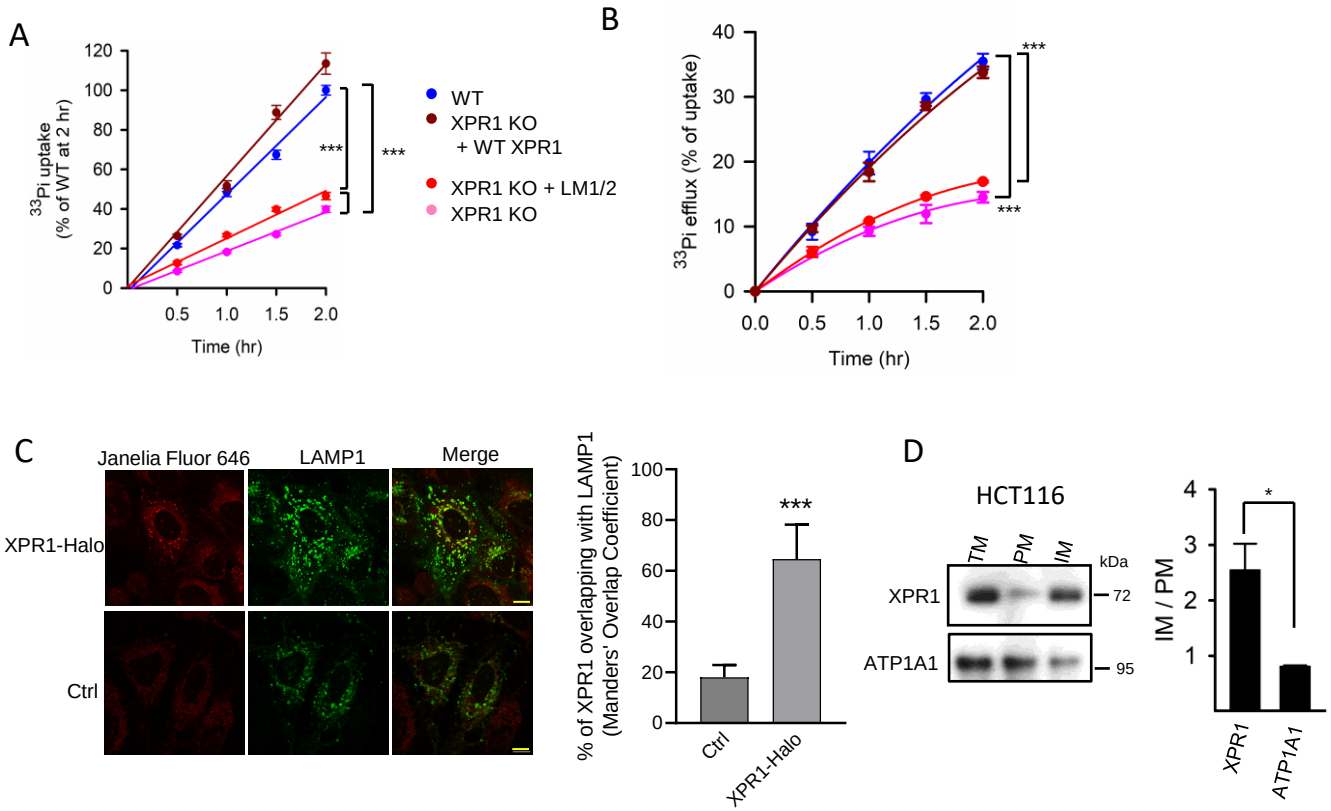

Figure S1. Organellar XPR1 regulates cellular phosphate fluxes, related to Figure 1. A, B, Time-courses of [^{33}P]-Pi uptake (A) and [^{33}P]-Pi efflux (B) respectively, in various strains of Saos-2 cells, color-coded as shown in a key below the graphs: WT (blue), XPR1 KO (pink), XPR1 KO + WT XPR1 (brown), XPR1 KO + the LM1/2 XPR1 mutant (red). **C**, Confocal analysis of live U2OS cells expressing endogenous XPR1-Halo, transfected LAMP1-GFP, and incubated for 4 hr in Pi-free medium and stained for 15 min with Halo-Janelia Fluor 646 immediately prior to imaging. The right panel provides a statistical analysis (Mander's coefficient) of the overlap of Halo-XPR1 with LAMP1 from 10 cells. Scale bars depict 10 µm. **D**, Membrane fractions were prepared from HCT116 cells (TM = total cell membrane fraction, PM = plasma membrane enriched fraction, IM = intracellular organelle membrane fraction) and analyzed by Western blots for XPR1, and the plasma membrane marker ATP1A1. The right-hand panel displays IM / PM ratios for each protein; data are means ± standard errors from 3 separate experiments. **, p = 0.017 (paired t-test).

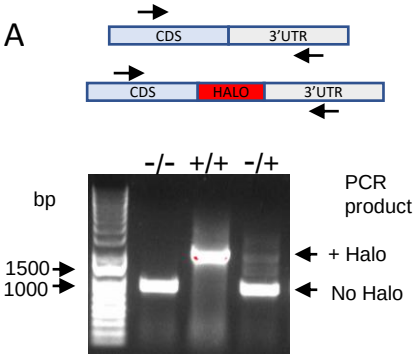

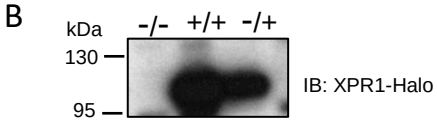

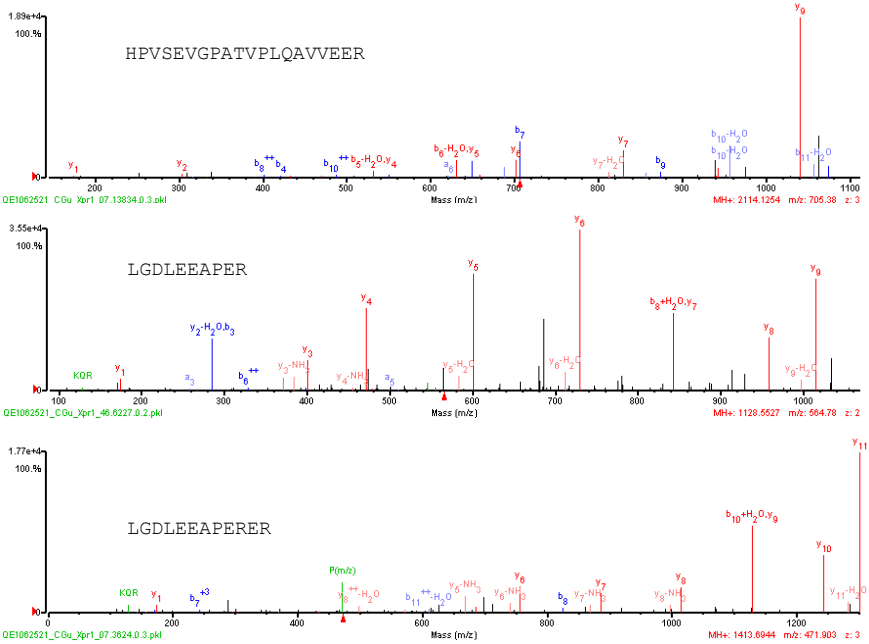

D

```
1   MATLITSTTA ATAASGPLVD YLWMLILGFI IAFVLAFSVG ANDVANSFGT AVGSGVVTLK
61  QACILASIFE TVGSVLLGAK VSETIRKGLI DVEMYNSTQG LLMAGSVSAM FGSAVWQLVA
121 SFLKLPISGT HCIVGATIGF SLVAKGQEGV KWSELIKIVM SWFVSPLLSG IMSGILFFLV
181 RAFILHKADP VPNGLRALPV FYACTVGINL FSIMYTGAPL LGFDKLPLWG TILISVGCAV
241 FCALIVWFFV CPRMKRKIER EIKCSPSESP LMEKKNSLKE DHEETKLSVG DIENK HPVSE
301 VGPATVPLQA VVEERTVSFK LGDLEEAPER ERLPSVDLKE ETSIDSTVNG AVQLPNGNLV
361 QFSQAVSNQI NSSGHYQYHT VHKDSGLYKE LLHKLHLAKV GDCMGDSGDK PLRRNNSYTS
421 YTMAICGMPL DSFRAKEGEQ KGEEMEKLTW PNADSKKRIR MDSYTSYCNA VSDLHSASEI
481 DMSVKAEMGL GDRKGSNGSL EEWYDQDKPE VSLLFQFLQI LTACFGSFAH GGNDVSNAIG
541 PLVALYLVYD TGDVSSKVAT PIWLLLYGGV GICVGLWVWG RRVIQTMGKD LTPITPSSGF
601 SIELASALTV VIASNIGLPI STTHCKVGSV VSVGWLRSKK AVDWRLFRNI FMAWFVTVPI
661 SGVISAAIMA IFRYVILRM
```

Figure S2. Proteomic identification of PiT1 in pulldowns of endogenous Halo-tagged XPR1, related to Figure 1. A, Graphic illustrating PCR amplification strategy of Halo-tagged *XPR1* gene and PCR product analysis in HCT116 cells. **B,** Western blot of Halo-tagged XPR1 using anti-Halo antibody. **C,** Mass spectrometry data for the indicated peptide fragments of PiT1. **D,** PiT1 sequence coverage.

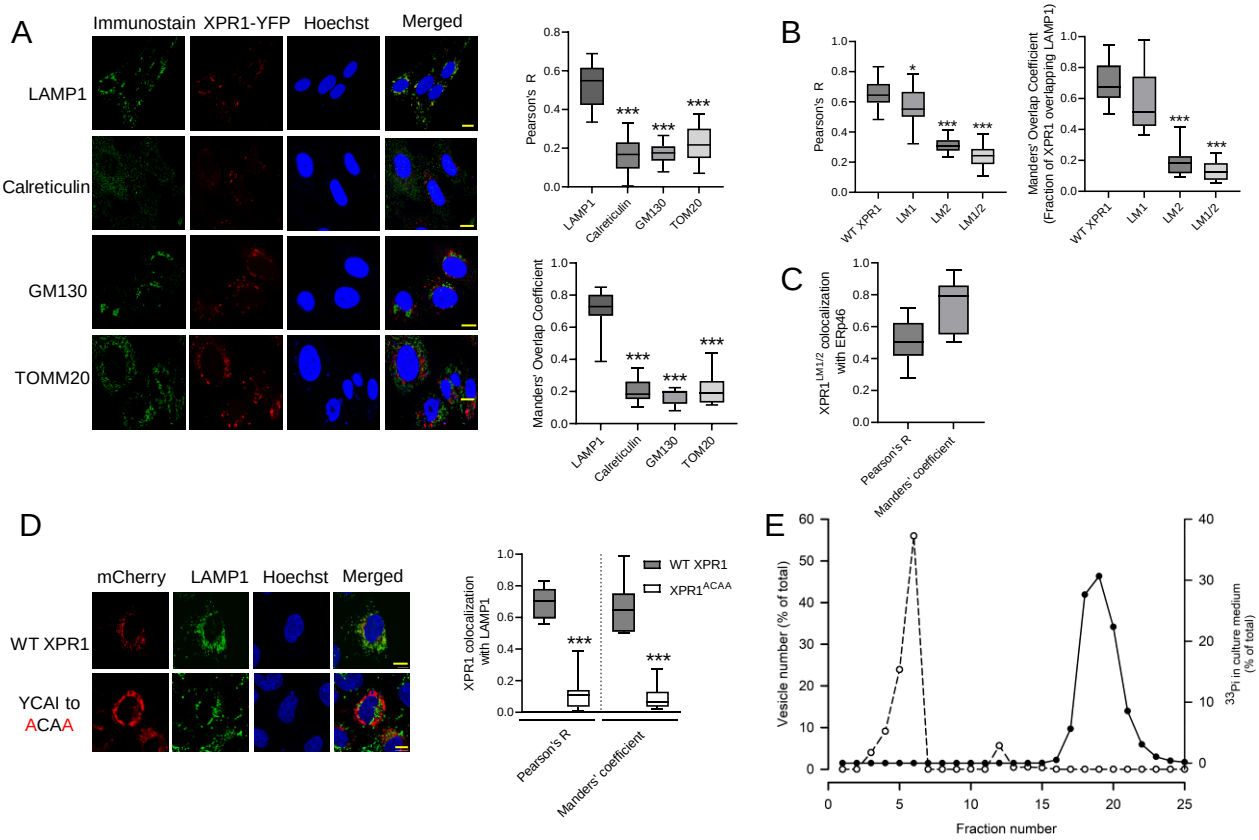

Figure S3. Analysis of intracellular location of XPR1 and extracellular vesicles in U2OS cells, related to Figure 1. **A,** Left panel, confocal analysis of U2OS cells transfected with XPR1-YFP and stained for either LAMP1, Calreticulin, GM130 or TOMM20. Right panels, statistical analysis of the Pearson's correlation coefficient (*R*) or Manders' coefficient for C-terminally YFP-tagged WT XPR1 with markers shown in left panel; data are means from analysis of 11-19 cells. ***, $p < 0.001$ (unpaired t-test). **B**, Statistical analysis of the impact of the Pearson's correlation coefficient (*R*) or Manders' coefficient for C-terminally mCherry-tagged WT XPR1 or mutants with LAMP1 (see Figure 1G); data are means from analysis of 11-22 images. ***, $p < 0.001$ (unpaired t-test). **C**, Pearson's coefficient (*R*) or Manders' coefficient for XPR1LM1/2 with ERp46 (See Figure 1H). **D**, Left panel, confocal analysis of U2OS cells transfected with either WT-XPR1 mCherry or the version hosting a mutation in the tyrosine-directed lysosomal motif (see Figure 1A); co-staining with anti-LAMP1 and Hoechst are also shown. Right panel, Pearson's coefficient (*R*) or Manders' coefficient analysis of the left panel; data are means from analysis of 11 images. ***, $p < 0.001$ (unpaired t-test). All scale bars depict 10 µm. **E**, Analysis of extracellular vesicles derived from media obtained from cultures of WT U2OS cells**,** Per radiation safety requirements, the vesicle analysis and [^{33}P] determinations were performed in parallel experiments. In each case, 0.5 ml of culture medium was collected from cells taken through a 2 hr duration Pi-efflux experiment (using either non-radioactive cultures or [^{33}P]-Pi labeled cultures). These samples were each fractionated into 250 µl aliquots on a qEV 35 size exclusion column (Izon.com) using phosphate-buffered saline as an eluate and a qEV Automatic Fraction Collector. The distribution of [^{33}P]-Pi (solid line with solid circle)was determined by liquid scintillation counting. Vesicle size and numbers (dash line with open circle) were assessed in 50 µl aliquots of each fraction using dynamic light scattering instrumentation (Zetasizer Ultra; Malvern Panalytical; ZEN2112 cell). The sizes of the particles were determined to be 30-200 nm.

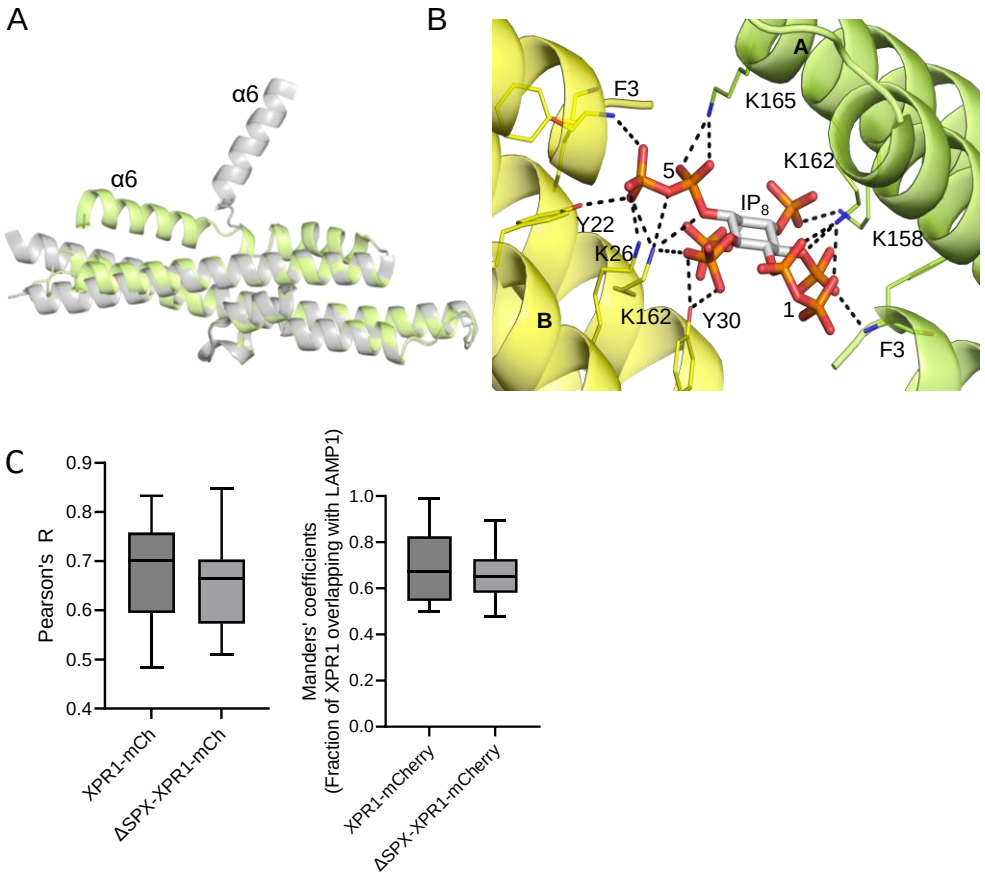

Figure S4. Structural and functional analysis of an SPX/IP_8 complex, related to Figure 2. A, Superimposition of ribbon plots of the apo-SPX domain of XPR1 (this study; lime-green) with the previously reported SPX/SO_4^{2-} crystal complex (PDB code, 5IJH; gray). **B**, Graphic showing the polar contacts (broken lines) involving two monomeric SPX molecules (ribbon plot, with key residues shown as stick models, where blue indicates nitrogen and orange indicates oxygen; monomer A is lime green, monomer B is yellow) and IP_8 (stick representation; gray = carbon, orange = phosphorous) after soaking the latter into preformed apo-SPX crystals. The two pyrophosphate groups of IP_8 (1 and 5) are numbered. **C**, Pearson's correlation coefficient (*R*) and Manders' coefficient for C-terminally mCherry-tagged WT XPR1 or ΔSPX-XPR1 colocalization with LAMP1 (see Figure 2B).

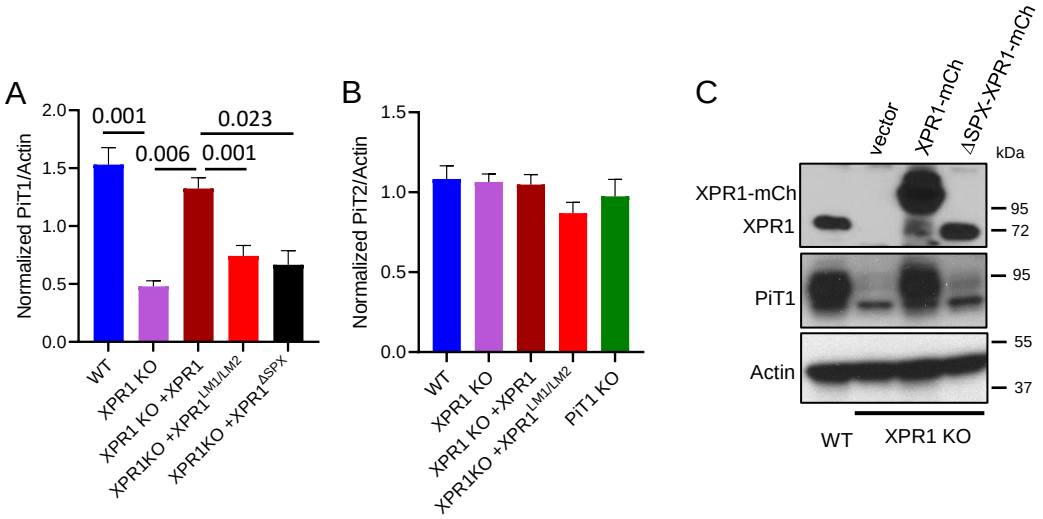

Figure S5. **PiT1 and PiT2 expression in U2OS cells, related to Figure 3. A, B**, Western blot quantification of PiT1 (**A**) or PiT2 (**B**) expression in the indicated strains of U2OS cells: WT, XPR1 KO, XPR1 KO + WT XPR1-mCherry, XPR1 KO + XPR1 LM1/LM2-mCherry and PiT1 KO (see Figure 3E); data shown are means and standard errors from 3 replicates. p values (paired t-test) of each comparison were added. **C**, PiT1 expression level in the following strains of U2OS cells: wild-type, and XPR1-KO cells stably transfected with either control vector, wild-type XPR1-mCherry, ΔSPX-XPR1-mCherry.

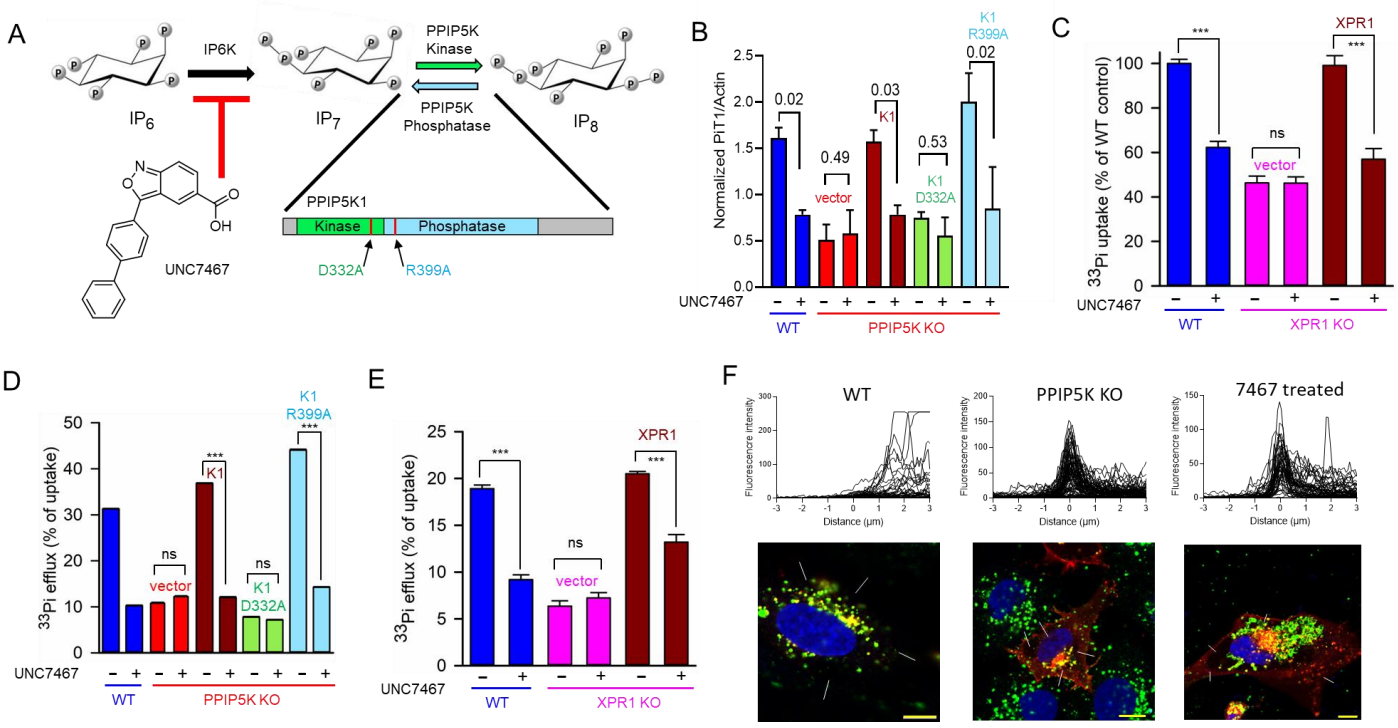

Figure S6. Effects upon Pi uptake, efflux and XPR1 localization following genetic and pharmacological manipulation of inositol pyrophosphate synthesis, related to Figure 3. A, Graphical depiction of pharmacological and genetic intervention in the pathway of IP_8 synthesis [1]. IP_6 is converted to IP_7 and then IP_8 by the sequential kinase activities actions of IP6K and PPIP5K1/2. IP6K activity is inhibited by cell treatment with UNC7467 [2]. PPIP5K1 (see domain graphic) and PPIP5K2 (not shown) each harbor distinct IP_7 kinase and IP_8 phosphatase activities; both enzymatic reactions are eliminated in PPIP5K KO cells, in which no IP_8 is synthesized [3]. In this study we also utilize our previously-described PPIP5K KO Saos-2 cell lines that host stable expression of either 1) WT PPIP5K1; 2) kinase-dead (D332A mutation) PPIP5K1; 3) phosphatase-dead (R399A mutation) PPIP5K1.[4] **B**, Western blot quantification of PiT1 levels in WT, PPIP5K KO, and PPIP5K KO Saos-2 cells stably expressing either WT PPIP5K1 or mutants, following treatment of cells for 6 hr with either 10 μM UNC7467 or DMSO vehicle (see Figure 3G); data shown are means and standard errors from 3 replicates. Specific p values of each comparison (paired t-test) were added. **C**, Total [^{33}P]-Pi uptake after 30 min of labeling, in WT or XPR1 KO U2OS cells, after treatment of cells for 6 hr with either 10 μM UNC7467 (see panel A) or DMSO vehicle. **D**, Total [^{33}P]-Pi efflux after 2 hr, as a percentage of [^{33}P]-Pi uptake, for WT, PPIP5K KO, and PPIP5K KO cells stably transfected with either vector control, PPIP5K1, or one of the indicated mutants, after treatment of cells for 6 hr with either 10 μM UNC7467 (see panel A) or DMSO vehicle. **E**, Total [^{33}P]-Pi efflux after 1 hr, as a percentage of [^{33}P]-Pi uptake, in WT or XPR1 KO U2OS cells, after treatment of cells for 6 hr with either 10 μM UNC7467 (see panel A) or DMSO vehicle. ***, $p<0.001$; ns = not significant. Two-way ANOVA, with Tukey's multiple-comparison test. **F**, Quantification of XPR1-mCherry fluorescence at the cell periphery. These experiments are replicates of data shown in Figure 3H. C-terminally mCherry-tagged WT XPR1 was expressed in either WT U2OS cells (left panel), PPIP5K KO U2OS cells (middle panel) or WT U2OS cells that had been treated for 6 h with 10 μM UNC7467 (right panel). The graphs depict relative XPR1-mCherry fluorescence intensities, which were calculated using ImageJ along 6 μm lines drawn perpendicular to the cell periphery (marked as zero on the x axis); these lines begin 3 μm inside the cell interior (positive distances) and end 3 μm into the extracellular space (negative distances). 11-21 images were analyzed. All scale bars depict 10 μm.

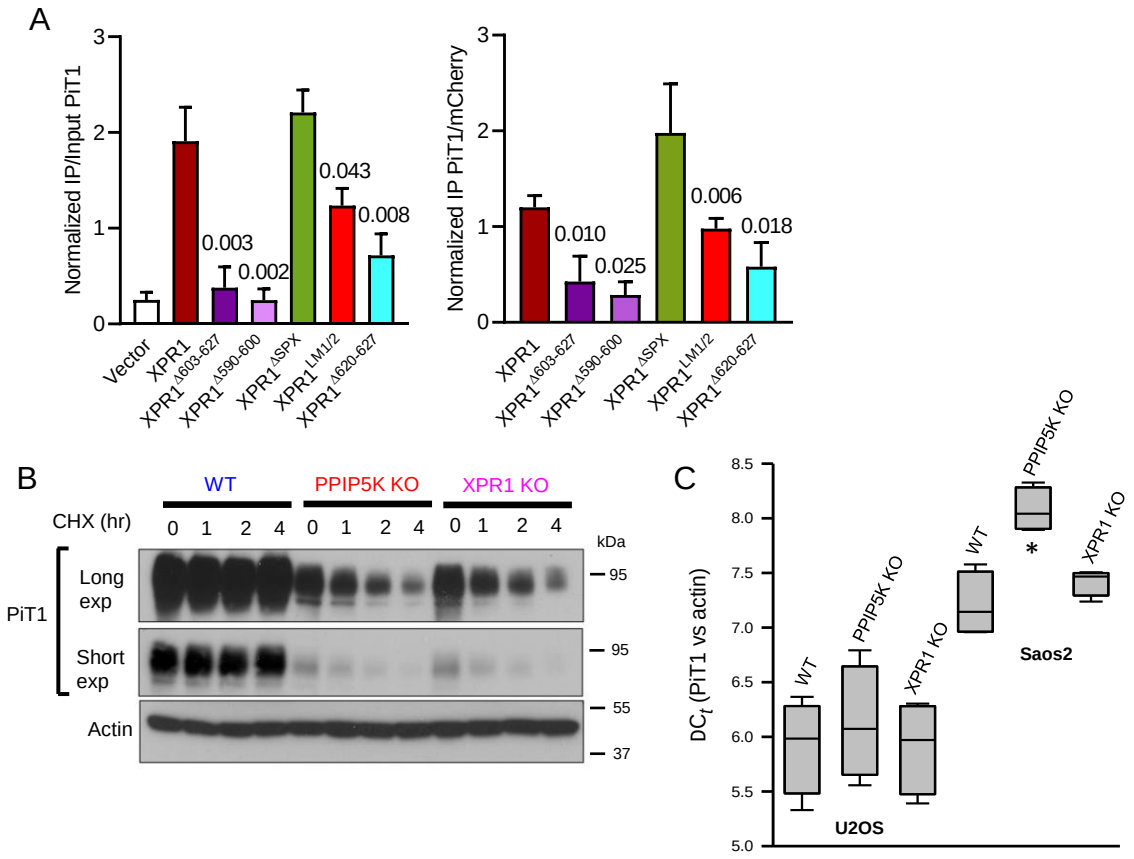

Figure S7. Analysis of PiT1 binding to XPR1 and its expression levels in U2OS or Saos-2 cells, related to Figure 4. A, Quantification of C-terminal mCherry tagged WT XPR1 or indicated mutants binding to PiT1 (see figure 4A) normalized to either Input PiT1 (left panel) **or** IP mCherry (right panel); data shown are means and standard errors from 3 replicates. P values (paired t-test) of each mutant comparing to WT XPR1 were added. **B**, Effects of cycloheximide on PiT1 protein expression in WT, PPIP5K KO and XPR1 KO cells. See Figure 4F in the main text for details. Data from two exposure times are shown for PiT1. **C**, PiT1 mRNA levels in WT, PPIP5K KO, and XPR1 KO U2OS or Saos2 cells; data shown are means and standard errors from 4 experiments. *, $p<0.05$ (paired t-test).

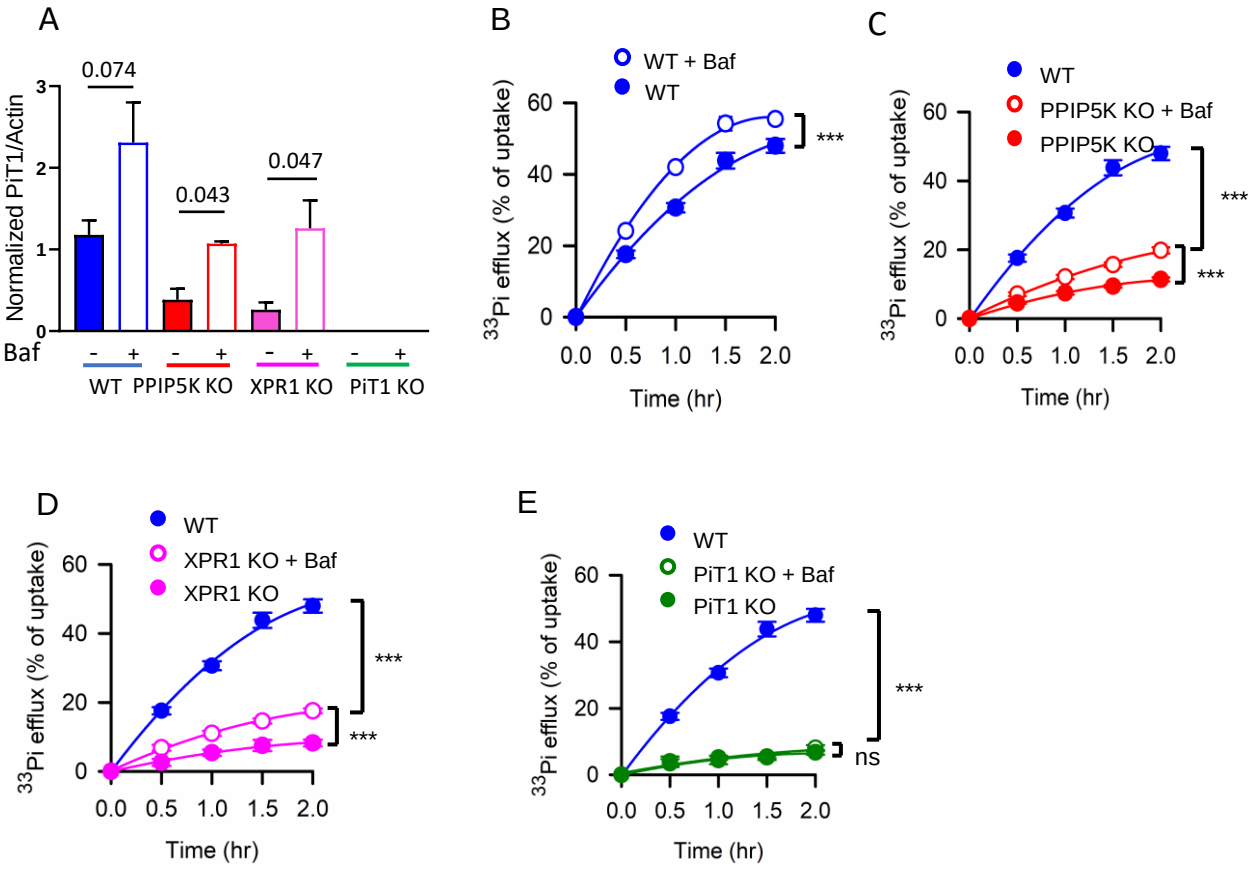

Figure S8. The effects of bafilomycin on Pi efflux, related to Figure 4. A, Quantification of PiT1 levels in U2OS cells treated with 50 nM Bafilomycin or DMSO vehicle as shown in Figure 1D. Data shown are means and standard errors from 3 replicates. P values (paired t-test) of each comparison were added. **B-D**, [^{33}P]-Pi efflux was recorded as a percentage of [^{33}P]-Pi uptake in the following strains of U2OS cells, incubated with and without overnight treatment with 50 nM bafilomycin: **B**, WT (these data are shown in the other panels to illustrate statistical analysis). **C**, PPIP5K KO. **D**, XPR1 KO. **E**, PiT1 KO. ***, p<0.001 two-way ANOVA, with Tukey's multiple-comparison test (zero time data excluded).

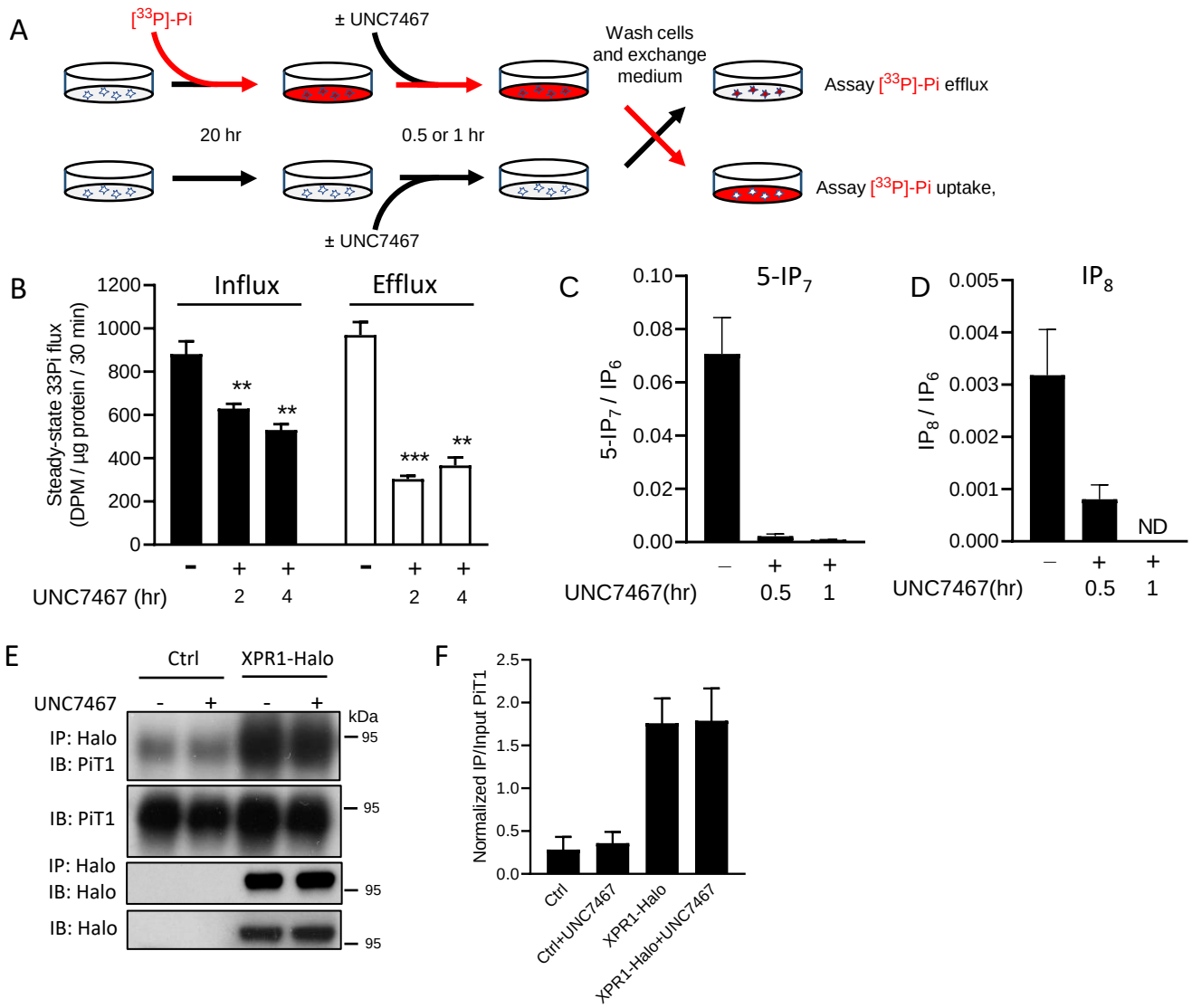

Figure S9. **The effects of UNC7467 upon steady-state cellular [^{33}P]Pi influx and [^{33}P]Pi efflux, related to Figure 5. A**, a graphical representation of the protocol. U2OS cells were seeded in 6 well plates at 4 x 10^5 cell/well and cultured for 24 h prior to addition of ~7.5uCi/ml [^{33}P]Pi to the medium and further cultured for 20 h. Parallel wells were cultured without [^{33}P]-Pi labeling. Cells were then incubated for a further 0.5, 1, 2 or 4 hr, with either 10 µM UNC7467 or DMSO vehicle control. Then the incubation media from labeled and unlabeled cells were removed and saved, and all cells were washed 4 x with DMEM. The radiolabeled medium was then added to the unlabeled cells to record [^{33}P]Pi-uptake, and the non-radiolabeled medium was added to the prelabeled cells to measure Pi efflux. All assays were terminated after 30 min. The cells that had not been prelabeled were washed 4 times with DMEM and lysed to measure Pi uptake. Protein concentration of the cell lysate was determined by BCA (Thermo-Fisher Scientific). **B**, Steady-state rates of [^{33}P]-Pi uptake and [^{33}P]-Pi efflux in WT U2OS cells treated for either 2hr or 4 hr with 10 µM UNC7467; data shown are means and standard errors from 4 biological replicates. **, p<0.01; ***, p<0.001, paired t-test. From the known amount of radioactivity added to the culture media, and by making the assumption that intracellular Pi does not significantly dilute the specific activity of the added [^{33}P]-Pi, and also assuming steady-state labeling conditions, we calculate that 1000 DPM is approximately equivalent to 0.08 nmol Pi. **C, D,** Levels of 5-IP_7 (**C**) or IP_8 (**D**) in U2OS cells treated with 10 µM UNC7467 for 0.5 or 1hr. Due to detection limits of IP_8, 6 replicates were combined into 2 samples (N=2) for each condition before measurement by CE-ESI-MS. ND = not detected. **E**, Immunoprecipitation of PiT1 by endogenous Halo-tagged XPR1 in HCT116 cells followed by 1h 10 µM UNC7467 treatment. **F**, Quantification of the XPR1 binding to PiT1 in panel E; data shown are means and standard errors from 3 replicates.

Supplementary Tables

Table S1. Excel sheet containing the list of binding proteins of endogenous Halo-tagged XPR1, related to Figure 1.

Table S2. Data collection and refinement statistics, related to Figure 2 and Structure analysis of the SPX domain in Method details.

PDB Accession IDs	8TYU	8TYV
	Apo	+IP8
Space group	$P2_1$	$P2_1$
Cell parameters *a*, *b*, *c* (Å);β	56.3, 47.8, 71.7; 107.5	56.7, 47.8, 70.4; 104.2
Resolution (Å)	50.0-1.30 (1.32)	50.0-1.85 (1.88)
Rmeas*	0.057 (0.690)	0.050 (0.670)
*I/σ I**	28.0 (2.2)	34.7 (2.1)
Completeness (%)*	97.2 (80.0)	98.2 (85.1)
Redundancy*	5.3 (3.9)	7.3 (5.5)
Refinement		
Resolution (Å)*	1.4 (1.45)	1.85 (1.92)
No. reflections	67810 (4979)	28423 (1689)
R_{work}*	0.165(0.191)	23.5 (29.2)
R_{free}*	0.202(0.248)	26.9 (37.7)
No. atoms		
Protein	2867	2828
Ligand/ion	N/A	44
Solvent	358	224
B-factors (Å^2)		
Protein	20.6	37.5
Ligand/ion	N/A	51.8
Solvent	33.0	37.9
R.M.S. deviations		
Bond length (Å)	0.008	0.010
Bond angle (°)	1.37	1.08
Ramachandran		
Favored (%)	98.6	98.2
Allowed (%)	1.4	1.8
Outliers (%)	0.0	0.00
Rotamer outliers (%)	0.0	0.00
Clashscore	3.5	6.9

*The numbers in parentheses are given for the highest-resolution shells.

Table S3: MS parameters for MRM transitions, related to Figure 5 and Quantification of Inositol pyrophosphates in Method details.

Molecular name	Precursor Ion	Product Ion	dwell	Fragmentor (V)	Collision Energy (V)	Cell Accelerator Voltage	Polarity
$[^{13}C_6]$ $InsP_6$	331.9	79.1	80	166	53	4	Negative
$InsP_6$	328.9	79.1	80	166	53	4	Negative
$[^{13}C_6]$ $InsP_7$	371.9	322.9	80	166	9	3	Negative
$InsP_7$	368.9	319.9	80	166	9	3	Negative
1,5$[^{13}C_6]$ $InsP_8$	411.9	362.8	80	166	9	1	Negative
1,5$InsP_8$	408.9	359.8	80	166	9	1	Negative

Reference

1. Randall, T.A., Gu, C., Li, X., Wang, H., and Shears, S.B. (2020). A two-way switch for inositol pyrophosphate signaling: Evolutionary history and biological significance of a unique, bifunctional kinase/phosphatase. Adv Biol Regul *75*, 100674.
2. Zhou, Y., Mukherjee, S., Huang, D., Chakraborty, M., Gu, C., Zong, G., Stashko, M.A., Pearce, K.H., Shears, S.B., Chakraborty, A., et al. (2022). Development of Novel IP6K Inhibitors for the Treatment of Obesity and Obesity-Induced Metabolic Dysfunctions. Journal of Medicinal Chemistry *65*, 6869-6887. 10.1021/acs.jmedchem.2c00220.
3. Gu, C., Nguyen, H.N., Ganini, D., Chen, Z., Jessen, H.J., Gu, Z., Wang, H., and Shears, S.B. (2017). KO of 5-InsP7 kinase activity transforms the HCT116 colon cancer cell line into a hypermetabolic, growth-inhibited phenotype. Proc. Natl. Acad. Sci. U. S. A *114*, 11968-11973.
4. Li, X., Gu, C., Hostachy, S., Sahu, S., Wittwer, C.J., Jessen, H.J., Fiedler, D., Wang, H., and Shears, S.B. (2020). Control of XPR1-dependent cellular phosphate efflux by InsP8 is an exemplar for functionally-exclusive inositol pyrophosphate signaling. Proc. Natl. Acad. Sci. U. S. A *117* (*7*), 3568-3574.